




 Cite this: *Lab Chip*, 2020, 20, 3815

Smart bio-gel optofluidic Mach–Zehnder interferometers multiphoton-lithographically customized with chemo-mechanical-opto transduction and bio-triggered degradation†

 Zhi-Shan Hou, ^a Yun-Lu Sun, ^{*b} Qi-Song Li,^{*c}
 Xudong Fan ^b and Rong Cheng^{*d}

Stimulus-responsive optical polymers, especially gels, are enabling new-concept energy-transducing “smart” optics. Full exploitation of their molecule-derived tuning and integration with traditional micro/nano-optics/optoelectronics rely on the implementation of devices by advanced “intelligent” micro/nano-manufacturing technologies, especially photolithographies with wide compatibility. In light of the increasing need for an organic combination of smart optical materials and digital micro/nano-manufacturing, novel “smart” optical micro-switches, namely, stimulus-actuated Mach–Zehnder interferometers as a proof-of-concept demonstration, were prototyped with protein-based hydrogels *via* aqueous multiphoton femtosecond laser direct writing (FsLDW). Protein-based Mach–Zehnder-interferometric smart optical devices here display a morphological quality sufficient for optical applications (average surface roughness $\leq \sim 20$ nm), nano-precision three-dimensional (3D) geometry of these millimeter-scale devices and purposely structured distribution of photo-crosslinking degree. Moreover, the device configuration was customized with unbalanced branches in which meticulous stimulus-responsive ability can be realized by simply tuning the surrounding chemical stimuli (*i.e.*, Na_2SO_4 concentration here). The “heterogeneous” configuration with unbalanced branches (*i.e.*, different optical and stimulus-responsive features) exhibits as-designed “smart” switching of propagated near-infrared light (~ 808 nm). These capabilities, along with total biodegradation, indicate the application promise of this gel-based optic construction strategy towards novel “intelligent”, bio/eco-friendly, self-tuning or sensing photonic integrated systems like optofluidics.

 Received 15th July 2020,
 Accepted 1st September 2020

DOI: 10.1039/d0lc00718h

rsc.li/loc

1. Introduction

Stimulus-responsive polymers, or more specifically, gel-based optics are drawing increasing efforts as a promising route to produce novel “smart” self-tuning optical systems with diverse features,^{1–3} such as simpler or even no tuning accessories, low cost, tailorable or adjustable mechanics, and bio/eco-compatibilities.^{4–8} The “smart” characteristics are

derived from the interior network of polymers or hydrogels permeated with modified side groups or molecules from the surroundings, which are “dually flexible” in terms of both mechanics and compositions or modifications.^{9,10} This makes them easy to endow with responses to stimuli, including optical, thermal, electrical, magnetic, chemical or biological signals, and enables devices to realize as-designed energy-transduction sensing or self-tuning.^{11–16} Implementing diverse characteristics and applications of hydrogel-based “smart” optics demands flexible and purposeful device construction with advanced manufacturing technologies to micro/nano-precisely and multi-dimensionally manipulate, process, and tailor the building blocks (*i.e.*, polymeric molecules) and their spatial organization,^{17,18} so that the “smart” energy-transductive capabilities can be effectively implemented by customizing device geometries and features (*e.g.*, refractive index, swelling response, *etc.*) structured as-needed to better manipulate light.^{19–21} Nevertheless, the current applications of smart polymer optical materials are still mostly based on simple structures such as homogeneous

^a State Key Laboratory of Precision Measurement Technology and Instruments, Department of Precision Instrument, Tsinghua University, Haidian, Beijing 100084, China

^b Department of Biomedical Engineering, University of Michigan, 1101 Beal Ave, Ann Arbor, MI 48109, USA. E-mail: yunlus@umich.edu

^c Key Laboratory of Materials for High Power Laser, Shanghai Institute of Optics and Fine Mechanics, Chinese Academy of Sciences, Shanghai 201800, China. E-mail: liqisong@siom.ac.cn

^d Department of Mechanical Engineering, Tsinghua University, Haidian, Beijing 100084, China. E-mail: chengr@tsinghua.edu.cn

† Electronic supplementary information (ESI) available. See DOI: 10.1039/d0lc00718h

membranes, single waveguides, and lenses.^{22,23} In our previous work we proposed nano-localized “heterogeneous” optical device configurations. For example, Y-junction micro/nano-elements have been realized to give full play to the intelligent optical response, sensing and tuning capabilities of the corresponding polymer/gel.²⁴ More specifically functionalized devices are still a challenge and have rarely been reported.

Herein, multi-photon lithography is used to construct a chemical-signal-responsive Mach–Zehnder-interferometric optical switch, which requires a 3D complex configuration design and difficult mesoscopic manufacturing at the nanometer to millimeter scale due to the need to select guiding modes.^{25–29} Biomacromolecules like proteins and their covalently or non-covalently formed gels swell or shrink, along with their geometrical and optical changes (*e.g.*, refractive index and light absorption), by actuating them with stimuli (*e.g.*, pH, ionic strength or other signals for specific proteins) through their responsive side-group electrostatics and molecular conformation.^{6,14} Based on femtosecond laser direct writing (FsLDW), a 3D heterogeneous preparation process for optical devices, this process can be customized with high precision and programmability.^{30–32} We applied an aqueous FsLDW of protein biomacromolecules (bovine serum albumin (BSA) here), optimized for one-step “printing” of micro/nano-devices with a large length–width ratio (over 1000 for a typical device with a length of ~ 5 mm and a line width of around 2–4 μm) and 3D high micro/nano-precision. Note that one important merit of this protein-hydrogel for bio-optics is its transmission window around near-infrared wavelengths, exactly in the optical window of human tissues and optical communications.³³ Thus it facilitates the integration of functional intelligent optical devices with existing commercial optical sensing and communication systems. A protein-based Mach–Zehnder-interferometric chemical sensor (P-MZIs) is produced with unbalanced branches as “smart” optical switches actuated by environmental signals (ionic strength here). The facilely programmable, noncontact and maskless “one-step” FsLDW^{34–36} has good biocompatibility and could adjustably retain the functions of proteins, showing flexible potential for further diverse functionalization and integration of P-MZIs. The long-range unbalanced P-MZIs was endowed with smooth morphology (average surface roughness of ~ 20 nm, meeting the requirements for optical applications), and sub-micrometer 3D spatial precision of the as-designed device geometry for accurate light manipulation. The two branches of unbalanced P-MZIs were fabricated with the same geometry, but different crosslinking degrees and therefore possessing heterogeneous refractive indexes and stimulus responses, by using localized FsLDW parameters. In addition, these unbalanced P-MZIs performed as “smart” optical switches actuated and triggered by environmental signals (*i.e.*, ion concentration for the demonstration here). This lithography-based strategy makes our method widely applicable, and it can be used to better develop various

polymers or hydrogel-based “smart” optics towards their practical construction into diverse, especially micro/nanoscale integrated, optical devices, for integration as functional parts in optic/photonic systems especially for optofluidics.^{37–40}

2. Experiments

In the experiment, the customized unbalanced P-MZIs was directly and facilely “written” out on magnesium fluoride film (deposited on a silicon wafer) from BSA ink (BSA, Sigma-Aldrich 600 mg mL⁻¹; rhodamine B, Aladdin, 2 mg mL⁻¹; ultrapure water, 18.2 M Ω cm, 25 °C) by FsLDW, as shown in Fig. 1a. The femtosecond laser pulses (ErFemto-780HP, width: 120 fs; repetition rate: 80 MHz) were focused on the sample by an objective lens (Olympus, NA = 0.75, 20 \times) (this lens is used instead of a higher magnification one to improve the processing efficiency as the structure is quite “huge” in terms of micro-bio-fabrication). The objective lens needed to be compensated by 0.17 mm, and this layer of glass can make the focused spot “tighter”. When the data file of the unbalanced P-MZIs was input into the fabrication program, three-dimensional air-bearing stages (Aerotech Inc.) moved relative to the sample in accordance with the trajectory. Two-photon absorption of RhB and tryptophan (Trp) occurred in the core region (Fig. 1a) during the scanning, then produced singlet oxygen ($^1\text{O}^2$), which induced redox polymerization of the residues of protein molecules. Through precise customization, the unbalanced P-MZIs arrays were conveniently prepared. Such fabrication was operated in a cavity sealed with aqueous ink. The micro/nano-devices were aqueously and inversely printed onto the surface of a ~ 5 μm -thick magnesium fluoride (MgF₂; RI = ~ 1.38) film on a silicon (Si) substrate. As the RI of the protein hydrogel is around ~ 1.47 (in air), the introduction of an MgF₂ layer improves RI matching and light propagation. The morphology and quality of the fabricated unbalanced P-MZIs were investigated with a scanning electron microscope (SEM) (JEOLJSM-7500F) and AFM (Veeco NanoScope). Fig. 1b shows the SEM characterization of unbalanced P-MZIs arrays, the lengths of which are more than 2.5 mm.

3. Results and discussion

A Mach–Zehnder interferometer (MZI) consists of a beam splitter (BS), two transmission waveguides and a beam combiner (BC), whose operating mechanism is shown in Fig. 1c. The input light is divided into two identical signals by the BS, which are then transmitted through the two transmission arms and finally merge together at the BC. Since the phase of the optical signal in each transmission arm can be changed, constructive interference will occur in the BC when the phase difference ϕ of the optical signals in the arms equals 0, that is, the intensity of the output and the input light intensity will be consistent in the ideal case. In contrast, when the phase difference $\phi = \pi$, destructive

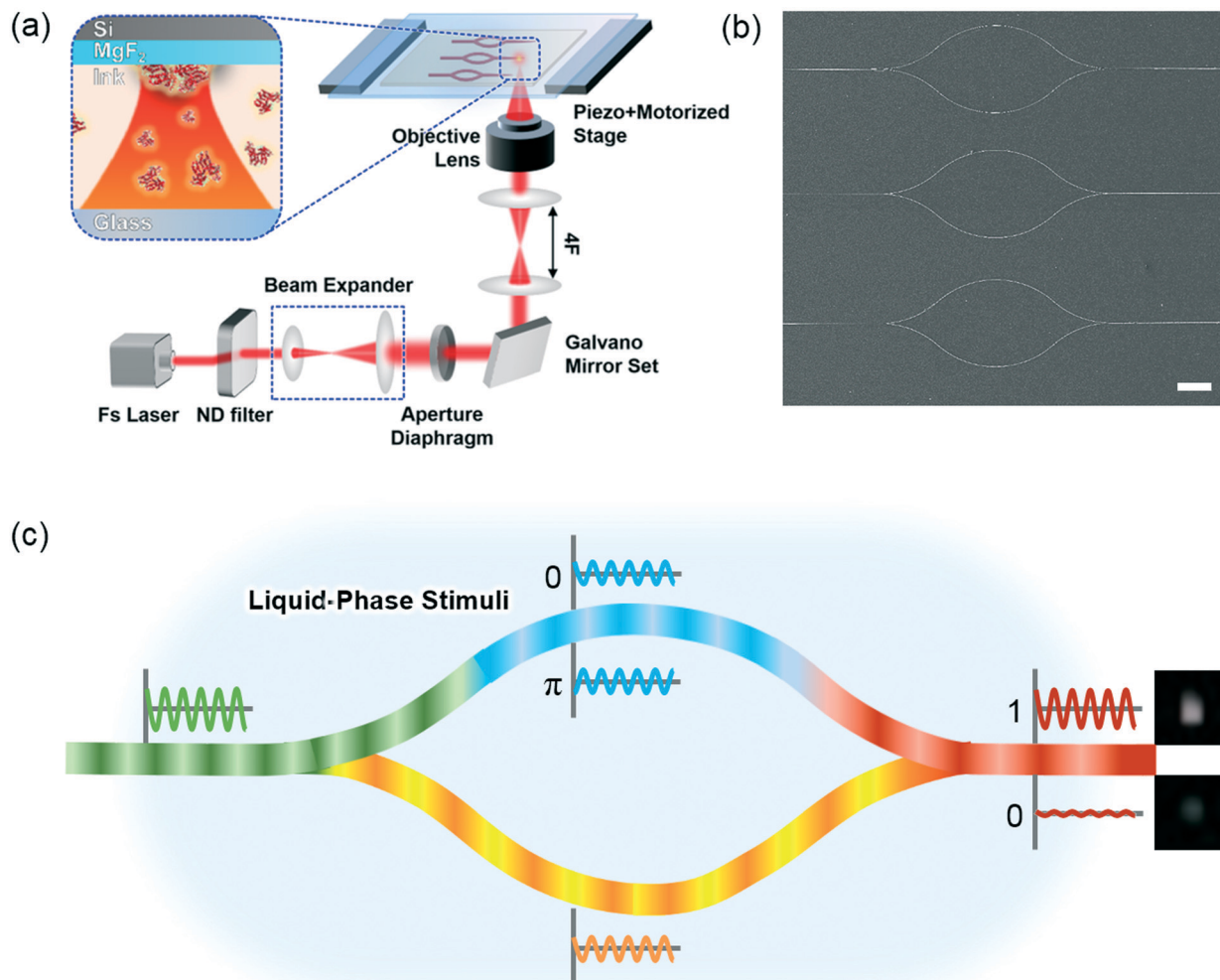


Fig. 1 (a) Schematic diagram of femtosecond laser processing system for preparing protein-hydrogel-based stimuli-responsive unbalanced Mach-Zehnder interferometric chemical sensor (unbalanced P-MZIs). Inset, detailed schematic of processing region. (b) SEM characterization of the unbalanced P-MZIs array; scale bar, 200 μm . (c) The operating principle of the Mach-Zehnder interferometer.

interference will occur and the central intensity of the output light is the weakest because of interference cancellation. Between these two extreme cases, the output light intensity will be changed due to the phase difference of the two arms. Thus, the propagation velocity of the light in the waveguides can be altered by adjusting the refractive index (RI) of one transmission arm, so that the phase difference can be changed when the light beam reaches the outlet to realize light intensity which is tunable and can be switched on or off.

Importantly, the energy cannot disappear, and the convergence of different phases of light at the BC will stimulate higher order modes. To minimize the number of guided modes in an unbalanced P-MZIs, the length and width of the waveguides at the outlet of the device are gradually decreased (as shown in Fig. 2a) by fully using two-photon absorption (the crosslinking occurs only in the tightly focused region) through decreasing the relative position between the focus region and the substrate. From the top

and side views, it can be seen that the height and width of the waveguides at the inlet and two arms are 2 μm and 4 μm while the size of the outlet slowly decreases from $4 \times 2 \mu\text{m}^2$ to $2 \times 0.15 \mu\text{m}^2$. Fig. 2b and c show a simulation of the P-MZIs with continuous reduction in the outlet size and constant size by the beam propagation method. In the simulation experiment of Fig. 2b, the RI of the waveguides is 1.40 (protein-hydrogel in water), and the waveguide is 1 mm in length with an initial width of 2 μm and an end width of 100 nm. In the light propagation process (from $z = 0 \mu\text{m}$ to $z = 1000 \mu\text{m}$), TE_0 , TE_1 , TE_2 , and TE_3 modes can all be transmitted in the waveguide during the inception phase. Then high-order modes begin leaking from the waveguide as the size of the waveguide gradually gets narrower and only the TE_0 mode can be transmitted in the end. The waveguide has a length of 1 mm, a width of 2 μm and remains constant in the simulation experiment of Fig. 2c, where all modes of light can be detected at the output this time. In an unbalanced P-MZIs, when the phase difference of the two

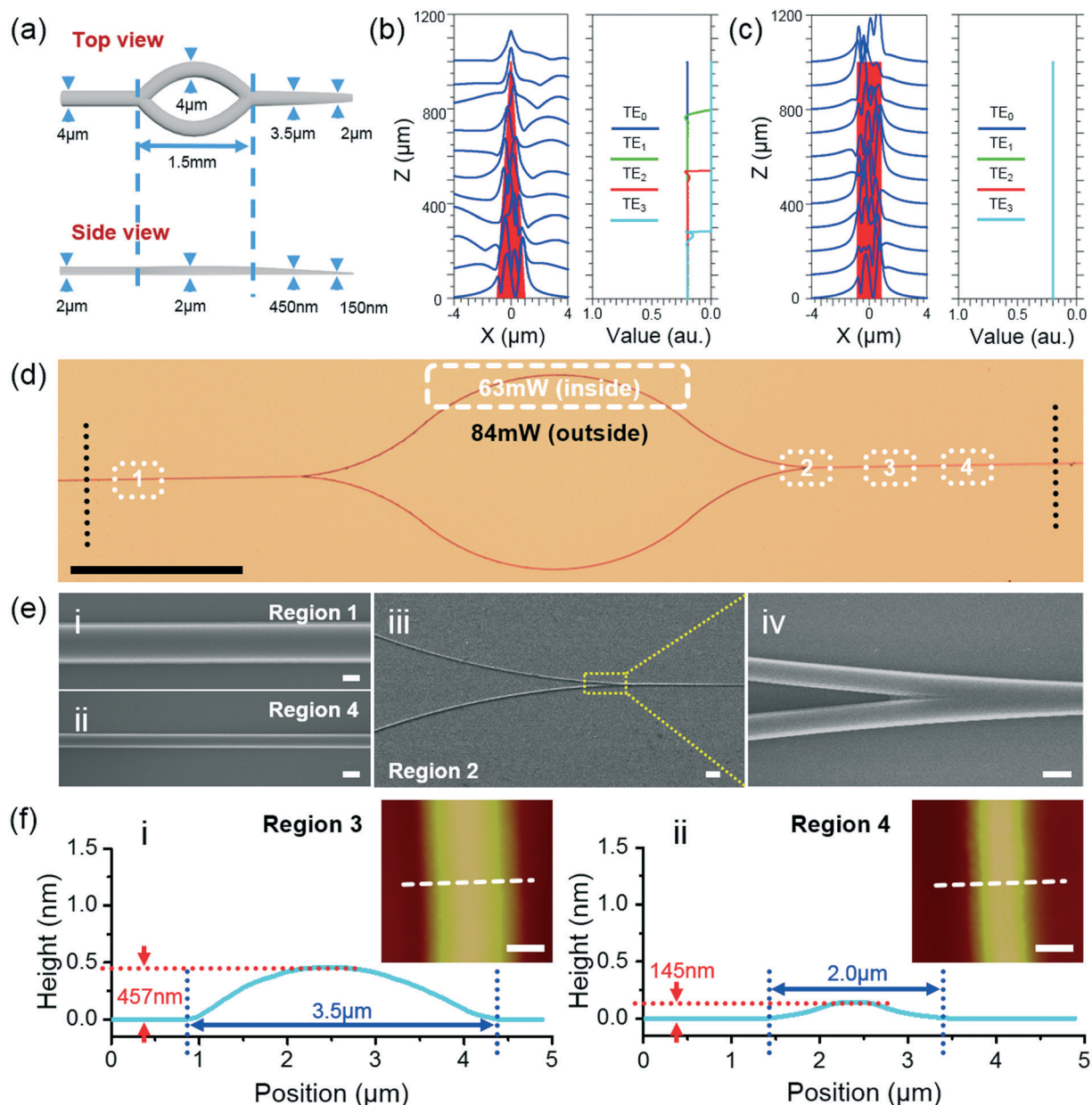


Fig. 2 (a) Top and side views of unbalanced P-MZIs. Rsoft simulation of the unbalanced P-MZIs with (b) continuously reducing outlet size and (c) constant outlet size. (d) Optical microscopic image of the protein-hydrogel-based stimuli-responsive unbalanced P-MZIs. (e) Enlarged-view SEM images corresponding to 1, 4, and 2 in (d). (f) AFM characterization of waveguide corresponding to 3 and 4 in (d). Inset: cross-section profiles; scale bars: (d) 0.5 mm, (e-i) and (e-ii) 2 μm, (e-iii) 10 μm, (e-iv) 5 μm, (f) 2 μm.

arms changes, the proportion of high order modes changes as well. As transmission of high order modes will not be supported by a single-mode waveguide, the light intensity will change.

Further, for an MZI, a light intensity transmission function could be determined from the following formula,

$$T_{\text{MZI}} = \frac{P_{\text{out}}}{P_{\text{in}}} = \frac{\left[\frac{\sqrt{2}}{2} (A_1 e^{j\varphi_1} + A_2 e^{j\varphi_2}) \right]^2}{A_1^2 + A_2^2} = \frac{1}{2} [1 + b \cos(\nabla\varphi + \varphi_0)]$$

$$\left(b = \frac{2A_1 A_2}{A_1^2 + A_2^2} \right)$$

where A_1 and A_2 represent the magnitude of the light in the two arms, φ_1 and φ_2 represent the phase-retardation in the arms, $\nabla\varphi$ and φ_0 correspond to the phase difference caused by extrinsic and intrinsic factors, respectively.

In this paper, the “heterogenization” of the unbalanced P-MZIs was delicately FsLDW-customized to realize the function of phase adjustment. It has been proved that a smaller FsLDW scanning step or higher scanning power would lead to higher RI of the protein-hydrogel.²⁴ As shown in Fig. 2d, the fabrication process was simple but efficient. At first, a waveguide with a length of 4 mm (for easy slicing) was

written out at a fabricating power of 84 mW before the objective lens. When writing the first arm, the attenuator (placed in the optical arm in advance) was adjusted slowly to make the power decrease to 63 mW and returned back to 84 mW before completing the arm. Then, a waveguide with a length of 3 mm was prepared when the relative position between the laser focus region and the substrate decreased. Finally, the second arm was written at a power of 84 mW. The scanning speed for the whole device was 0.1 mm s^{-1} . In this way, the customized unbalanced P-MZIs was readily fabricated in 2 minutes. The prepared samples were then cut carefully (especially for the outlet for single mode transmission). Fig. 2e shows the enlarged-view SEM images corresponding to regions 1, 4, and 2 in Fig. 2d. It can be seen that the device has a good appearance and the surface of the device is smooth and the connection at the bifurcation shows no obvious defects. The AFM characterization in Fig. 2f and g shows that the waveguide in region 4 is smaller than that in region 3 both in height and width, which means the P-MZIs can conform well to the anticipated designs.

The protein molecules contain a large number of ionizable groups (*e.g.* amino groups and carboxyl groups). When immersed in water, the ionization of these groups and the change in their electrostatic states will lead to swelling or shrinking of the protein molecules. The ionization degree of these groups can be adjusted by changing the pH value or ion concentration in the aqueous solution, so that the equilibrium swelling of these protein micro/nano-hydrogels can be manipulated. Furthermore, the “heterogeneous” arms are constructed with different crosslinking densities, and therefore different degrees of swelling or shrinking occur even under the same environmental conditions. Consequently, the optical performances and waveguide cross-section geometry have different stimulus responses in the two branches of an unbalanced P-MZIs.

To analyze the RI changes of the protein-hydrogel in the two arms, Rsoft simulations were performed with the beam-propagation mode on the typical P-MZI configurations ($2 \mu\text{m}$ line width) in an aqueous environment (Fig. 3). The RI of as-formed protein hydrogel is set to 1.40 in pure water according to previous work, and the surrounding RI is 1.33 (water).

In Fig. 3a, both arms have the same RI (1.40), which means the entire device has been fabricated by FsLDW with constant parameters to produce symmetrical branching waveguides in terms of both RI distribution and device structure. A unit of light was coupled in the P-MZIs and the detector located at the end of the device detected light with a relative light intensity of 1 unit, which means that the light switch was turned on in that situation. In the simulation experiment in Fig. 3b, the RI of the two arms are 1.40 and 1.402, respectively, and the detector detected light with a relative value of 0, that is, no signal was detected, and the light switch was turned off.

In the simulation experiment in Fig. 3c, the RI is 1.40 for one arm, and $1.40 + \Delta n$ for the other one. Fig. 3c shows the

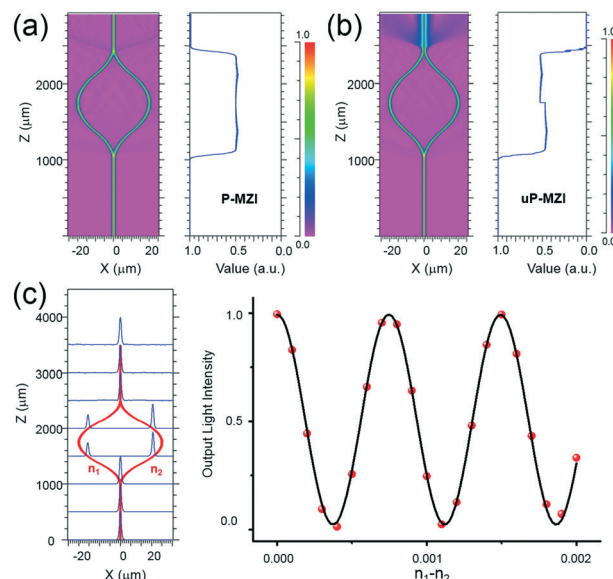


Fig. 3 Rsoft simulation of a (a) P-MZI and (b) unbalanced P-MZIs (uP-MZIs, high order mode light is generated and escapes from waveguides). (c) Rsoft simulation of unbalanced P-MZIs, output light intensity along with Δn increasing from 0.0 to 0.005; n_1 and n_2 represent RI of the 84 mW power FsLDW arm and 63 mW power FsLDW arm, respectively.

output light intensity of an unbalanced P-MZI sensors when Δn increases from 0.0 to 0.005. The n_1 , n_2 denote the RI of the arms in pure water with higher processing power (arm 1) and lower processing power (arm 2), respectively. It can be seen that as the RI difference between the two arms increases, the output light intensity is a sinusoidal oscillation signal. There is no doubt that n_1 is slightly larger than n_2 in pure water due to its denser crosslinking, and when the salt concentration increases from 0 mol L^{-1} , a greater increase in the RI of arm 2 results in a decrease in Δn . Compared with other tunable switches, the unbalanced P-MZIs possesses new chemical stimuli responding to “smart” adjustments, as well as fine “configurability” through simple manufacturing and structural changes.

With 808 nm light propagation, the interference behaviour of the PMZIs in pure water was observed by a CCD, as schematically illustrated in Fig. 4a. In Fig. 4b, a P-MZIs (two arms were fabricated with the same parameters) was tested with approximately constant output light intensities. The output intensity decreased linearly during the process of tuning the surrounding Na_2SO_4 concentration from 0 mol L^{-1} to $18 \times 10^{-3} \text{ mol L}^{-1}$. In detail, the salt solution of each concentration was preconfigured and titrated on the substrate to immerse both arms. Importantly, the device was softly flushed with continuous water for 30 s and then dried before the signal of the next concentration was measured. Integrating the output light intensity collected by the CCD (the gray values were accumulated and normalized as the indexes of output intensities), the calculated interference loss for the P-MZIs is about $0.0615 \text{ dB mol}^{-1} \times \text{L}^{-1}$. Such a loss might be caused by shrinking of the protein-hydrogel which

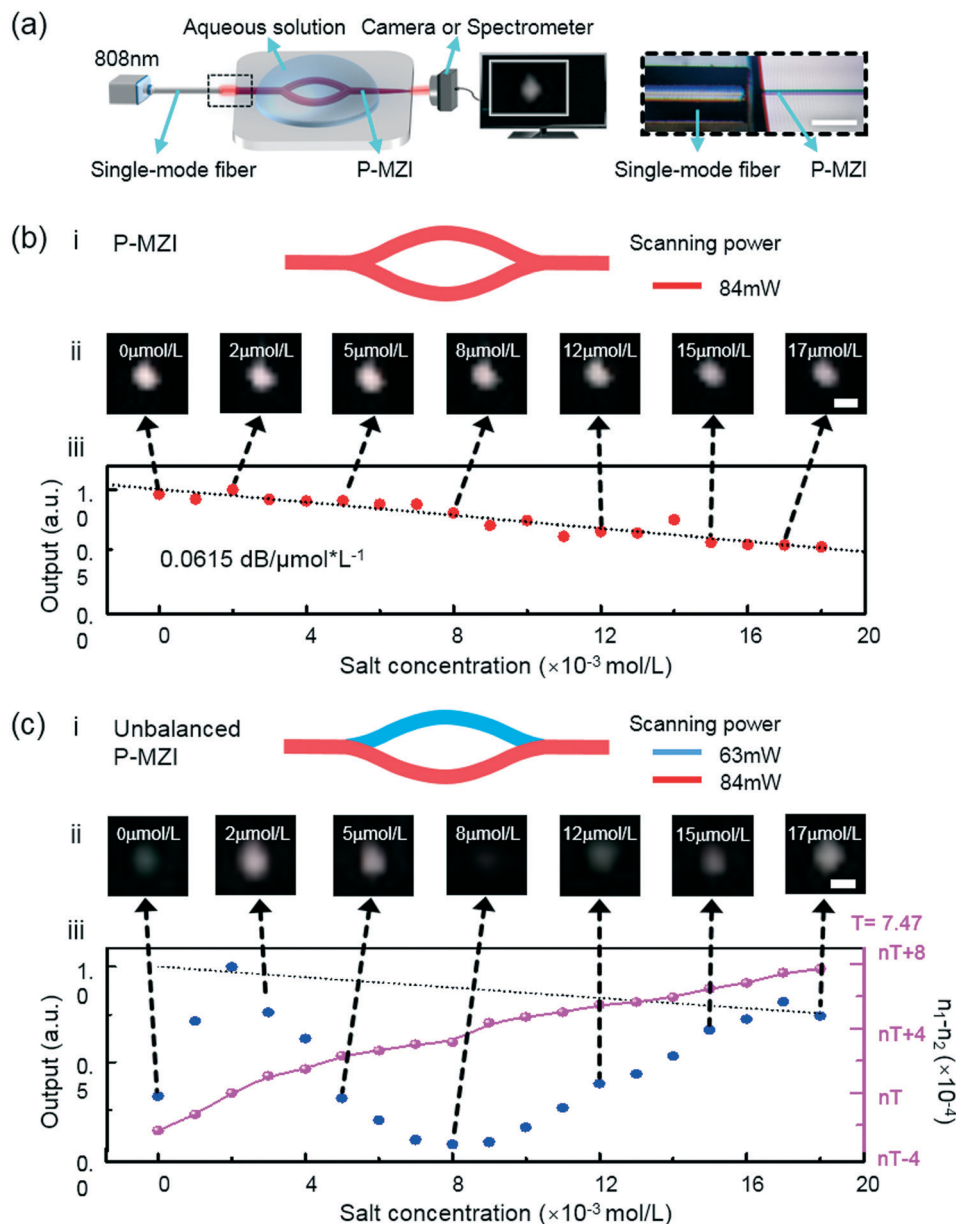


Fig. 4 (a) Schematic of the test of an unbalanced P-MZIs; scale bar, 50 μm. (b and c) Output light intensity of a (b) P-MZIs and (c) unbalanced P-MZI along with Na₂SO₄ concentration increasing vs. 808 nm light launched and propagated. ii: Dark-field OM images; scale bars, 200 nm. iii: The red and blue dots represent the relative values of the measured light intensity; the black dotted line represents the fitted transmission loss; the purple dots and lines represent the calculated RI difference between the two arms of the unbalanced P-MZI.

led to an increase in surface roughness that induced more leakage of light during propagation, and increased the transmission loss as a result. Similar tests were carried out using the unbalanced P-MZIs in Fig. 4c. This shows that with the Na₂SO₄ concentration rising from 2×10^{-3} to 8×10^{-3} mol L⁻¹, the unbalanced P-MZIs realized the entire operation of an optical switch. In other words, such a sensor can be a light intensity actuator. The insets in Fig. 4bc and show a set of dark-field OM (optical microscope) images of the output light of the samples (see details in ESI† Fig. S1). The purple dots represent the calculated RI difference between the two arms of the unbalanced P-MZI. As the efficiency of the

equilibrium shrinkage of the arms diminished along with a further increase in Na₂SO₄ concentration, the light “off” operation ($2\text{--}8 \times 10^{-3}$ mol L⁻¹) was faster than the light “on” ($8\text{--}17 \times 10^{-3}$ mol L⁻¹) operation.

Additionally, surrounding chemical signals (pH value, salt concentration) should cause greater changes in protein-hydrogel than possible temperature changes,²⁴ and the results of the comparative experiment also demonstrated that the operation of the light was due to changes in the ion concentration in the solution. Meanwhile, relatively low-energy input light, and aqueous environments in this experiment should be helpful for heat dissipation. Notably,

there is a very significant character of protein-hydrogels that they can be soluble by enzymes. The enzymatic hydrolysis principle and experiments on protein-hydrogels were tested, and Fig. 5 shows the results. In the effect of enzymatic hydrolysis, the chemical bond between the protein-hydrogel is broken and the OH⁻ is introduced into the C-N bond and the H⁺ to the C, which are obtained from the water-resolved molecules. Then the BSA protein-hydrogel is disassembled to peptide and amino acid which can be dissolved in the water just as in the process shown in Fig. 5a. For the convenience of observation, the sample was prepared with a length of about 70 μm and the cross section of the waveguide is 4 × 2 μm². After mixing proteinase K with phosphate buffer saline (PBS) into a 1 mg ml⁻¹ solution, the sample was immersed in it at 58 °C (proteinase K is active at this temperature) and the results are shown in Fig. 5b. After timing for one minute, the sample was lifted out gently and dried completely at room temperature. Then the dissolution of the sample with a fluorescence microscope was observed, and it was put it back

into the solution. In this way, the protein-hydrogel could be removed well and completely hydrolyzed in 1 h (details in ESI†). Fig. 5c shows a comparative test under the same conditions (PBS solution without proteinase K).

Although the unbalanced PMZIs had been successfully prepared, the current transmission loss (~25 dB cm⁻¹) is too large for further expansions and applications, especially when higher integration and inter-chip interconnection are required. In our opinion, in addition to the absorption loss of light by protein materials, the main cause of energy loss is that the molecular mass of the protein is large and the side chains are complex. By flexible design, there is one way to minimize the transmission loss of the device. For example, protein-hydrogel can be used in the critical sensing areas of the devices, while the remaining areas still use a mature commercial photoresist or other low-loss materials. Such a design could add the desired sensing mechanism with minimal interference with device performance, which is also the focus of our future work.

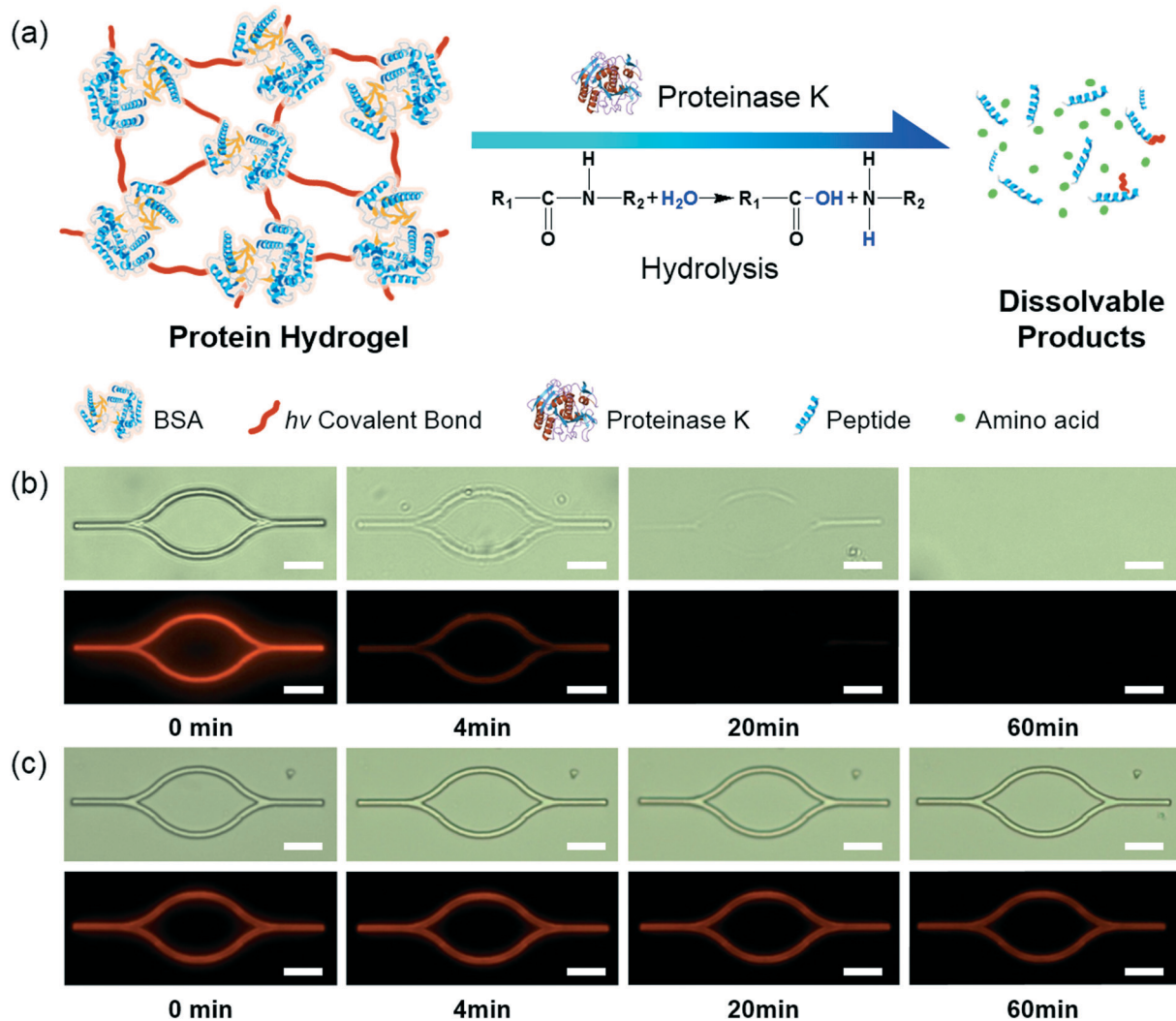


Fig. 5 (a) The hydrolysis principle of protein-hydrogel in proteinase K. (b) The proteinase K digestion test with protein-hydrogel. (c) The protein-hydrogel in phosphate-buffered saline (PBS). Scale bars, 10 μm.

4. Conclusions

In summary, we have reported a distinctive method to customize functional optofluidic devices (*i.e.*, P-MZIs here) with 3D configuration and nano-precision details by flexibly using FsLDW and smart optical polymers/gels. It is “scalable” to the construction of various polymer or gel based energy-transductive smart optics. The facilely programmable, noncontact and maskless “one-step” FsLDW guarantees the customization of the flexible device with a nano-level quality of morphology and geometry while the biological or chemical properties of the protein-hydrogels are controllably preserved (*i.e.*, stimuli responses, biodegradation, *etc.*). To manipulate the propagation of light at ~ 808 nm as designed, the protein-based waveguides were customized with 3D profiles that gradually and continuously vary with a total height change of ~ 1.85 μm (2 μm to 150 nm) across the ~ 2 mm device length. Meanwhile, by tailoring the multiphoton crosslinking inside the micro/nano-gels, the device configuration was fabricated with “unbalanced” branches with the same geometry but purposely different refractive indexes and stimulus-responsive shrinking/swelling features. Therefore, the devices can be endowed with 3D configurations in both the “external” three-dimensional structure and the “internal” three-dimensional material characteristic distribution as needed (*i.e.*, “dual 3D”). The unbalanced P-MZIs exhibit a dynamically tuned difference of the effective path length in the two branches, and “smart” optical adjustments and switching under actuation/stimulation in an aqueous fluidic environment. Furthermore, it can be totally biodegraded with the help of protease in the aqueous phase. Protein-based micro/nano-devices including optics here provide higher flexibility and better convenience for modification and functionalization with probing molecules like antibodies for specific biomolecule responses and signal-opto-transductions with specific molecules compared with existing liquid optofluidic Mach-Zehnder interferometers. This work demonstrates a versatile method to “intelligently” construct gel-based micro/nano-optics and makes full use of their molecular energy transduction and “smart” adjustments towards novel self-tuning or sensing integrated optics and photonics (*e.g.*, optofluidics).

Conflicts of interest

There are no conflicts to declare.

Acknowledgements

This work was supported by the National Science Foundation of China (61590930, 61235003, 61905263), Science Foundation for Youths (61605055), China Postdoctoral Science Foundation Funded Project (801161010428), Shanghai Sailing Program (Grant No. 18YF1426300).

References

- Z. Wu, X. Chen, M. Wang, J. Dong and Y. Zheng, *ACS Nano*, 2018, **12**, 5030–5041.
- A. S. Kuenstler, H. Kim and R. C. Hayward, *Adv. Mater.*, 2019, **31**, 1901216.
- Z. Zhang, J. Pan, Y. Tang, Y. Xu, L. Zhang, Y. Gong and L. Tong, *Lab Chip*, 2020, **20**, 2572–2579.
- S. Iamsaard, E. Villemin, F. Lancia, S. J. Aßhoff, S. P. Fletcher and N. Katsonis, *Nat. Protoc.*, 2016, **11**, 1788–1797.
- D. R. Morim, A. Meeks, A. Shastri, A. Tran and K. Saravanamuttu, *Proc. Natl. Acad. Sci. U. S. A.*, 2020, **117**, 3953–3959.
- S. Nocentini, D. Martella, C. Parmeggiani, S. Zanotto and D. Wiersma, *Adv. Opt. Mater.*, 2018, 1800167.
- S. Palagi, D. P. Singh and P. Fischer, *Adv. Opt. Mater.*, 2010, **7**, 1900370.
- M. Yao, O. Xia, J. Wu, A. Zhang, T. Hwa-Yaw and P. Wai, *Sensors*, 2018, **18**, 1825.
- H. Kim, J.-H. Kang, Y. Zhou, A. S. Kuenstler, Y. Kim, C. Chen, T. Emrick and R. C. Hayward, *Adv. Mater.*, 2019, **31**, 1900932.
- X. Liu, H. Gao, J. E. Ward, X. Liu, B. Yin, T. Fu, J. Chen, D. R. Lovley and J. Yao, *Nature*, 2020, **578**, 550–554.
- N. Bodenberger, D. Kubiczek, I. Abrosimova, A. Scharm, F. Kipper, P. Walther and F. Rosenau, *Biotechnol. Rep.*, 2016, **12**, 6–12.
- L. Zhang and Z. Xu, *J. Cleaner Prod.*, 2016, **127**, 19–36.
- P. Y. Chen, J. Mckittrick and M. A. Meyers, *Prog. Mater. Sci.*, 2012, **57**, 1492–1704.
- M. Jo, K. Min, B. Roy, S. Kim, S. Lee, J. Y. Park and S. Kim, *ACS Nano*, 2018, **12**, 5637–5645.
- S. Kapoor and S. C. Kundu, *Acta Biomater.*, 2015, **31**, 17–32.
- H. Xiao, P. Cebe, A. S. Weiss, F. Omenetto and D. L. Kaplan, *Mater. Today*, 2012, **15**, 208–215.
- J. Feng, Q. Jiang, P. Rogin, P. W. de Oliveira and A. del Campo, *ACS Appl. Mater. Interfaces*, 2020, **12**, 20287–20294.
- Y. L. Sun, H. Y. Tang, A. Ribbe, V. Duzhko, T. L. Woodard, J. E. Ward, Y. Bai, K. P. Nevin, S. S. Nonnenmann, T. Russell, T. Emrick and D. R. Lovley, *Small*, 2018, **14**, 1802624.
- T. Nakaji Hirabayashi, K. Kato and H. Iwata, *Biomacromolecules*, 2008, **9**, 1411–1416.
- M. H. Tong, N. Huang, W. Zhang, Z. L. Zhou, A. H. W. Ngan, Y. Du and B. P. Chan, *Sci. Rep.*, 2016, **6**, 20063.
- R. Xiong, J. Luan, S. Kang, C. Ye, S. Singamaneni and V. V. Tsukruk, *Chem. Soc. Rev.*, 2020, **49**, 983–1031.
- B. Dong, H. Li, Z. Zhang, K. Zhang, S. Chen, C. Sun and H. F. Zhang, *Optica*, 2015, **2**, 169–176.
- K. Tsioris, G. E. Tilburey, A. R. Murphy, P. Domachuk, D. L. Kaplan and F. G. Omenetto, *Adv. Funct. Mater.*, 2010, **20**, 1083–1089.
- S. M. Sun, Y. L. Sun, B. Y. Zheng, P. Wang, Z. S. Hou, W. F. Dong, L. Zhang, Q. D. Chen, L. M. Tong and H. B. Sun, *Sens. Actuators, B*, 2016, **232**, 571–576.
- T. Berrada, S. Van Frank, R. Bücken, T. Schumm, J. F. Schaff and J. Schmiedmayer, *Nat. Commun.*, 2013, **4**, 2077.
- K. Misiakos, A. Botsialas, I. Raptis, E. Makarona, P. Petrou, S. Kakabakos, G. Jobst, R. Stoffer and M. Hoekman, *Sensors*, 2011, 1317–1320.

- 27 M. H. Lee, Y. H. Min, J. J. Ju, J. Y. Do and S. K. Park, *IEEE J. Sel. Top. Quantum Electron.*, 2001, **7**, 812–818.
- 28 Y. Ji, C. Y. C. D. Sprinzak, M. Heiblum, D. Mahalu and H. Shtrikman, *Nature*, 2003, **422**, 415–418.
- 29 P. Lu and Q. Chen, *Electron. Lett.*, 2010, **46**, 1616–1617.
- 30 Y. L. Sun, Q. Li, S. M. Sun, J. C. Huang, B. Y. Zheng, Q. D. Chen, Z. Z. Shao and H. B. Sun, *Nat. Commun.*, 2015, **6**, 8612.
- 31 L. Jiang, A. D. Wang, B. Li, T. H. Cui and Y. F. Lu, *Light: Sci. Appl.*, 2018, **7**, 17134.
- 32 D. Pavlov, A. Zhizhchenko, M. Honda, M. Yamanaka, O. Vitrik, S. Kulinich, S. Juodkazis, S. Kudryashov and A. Kuchmizhak, *Nanomaterials*, 2019, **9**, 1348.
- 33 L. Meng, J.-h. Yin, Y. Yuan and N. Xu, *Anal. Methods*, 2017, **9**, 768–773.
- 34 F. Guo, A. Karl, Q. F. Xue, K. C. Tam, K. Forberich and C. Brabec, *Light: Sci. Appl.*, 2017, **6**, e17094.
- 35 S. Syubaev, E. Mitsai, A. Porfirev, S. Khonina, S. Kudryashov, T. Katkus, S. Juodkazis, E. Gurevich and A. Kuchmizhak, *Opt. Lett.*, 2020, **45**, 3050–3053.
- 36 Z. Qian, Y. Dong, Q. Jia, C. Ya, G. Qihuang and L. Yan, *Opt. Express*, 2017, **25**, 13263–13270.
- 37 S. Waheed, J. M. Cabot, N. P. Macdonald, T. Lewis, R. M. Guijt, B. Paull and M. C. Breadmore, *Lab Chip*, 2016, **16**, 1993–2013.
- 38 F. Sima, K. Sugioka, R. M. Vázquez, R. Osellame, L. Kelemen and P. Ormos, *NANO*, 2018, **7**, 613–634.
- 39 J. Zhu, X. Zhu, Y. Zuo, X. Hu, Y. Shi, L. Liang and Y. Yang, *Opto-Electron. Adv.*, 2019, **2**, 190007.
- 40 J. Zhu, G. Han, X. Hu, Y. Zuo and X. Han, *ACS Sens.*, 2020, **5**, 1381–1388.